Nanoscale

Accepted Manuscript

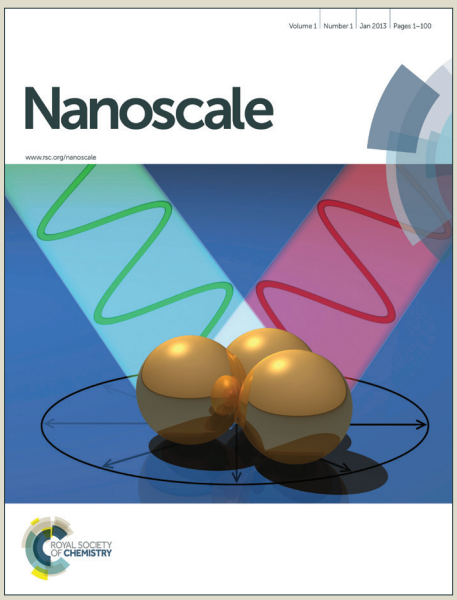

ROYAL SOCIETY OF CHEMISTRY

www.rsc.org/nanoscale

Journal Name

RSCPublishing

ARTICLE

Length Scale of Leidenfrost Ratchet Switches Droplet Directionality

Cite this: DOI: 10.1039/xoxxoooooox

Received ooth January 2012,
Accepted ooth January 2012

DOI: 10.1039/xoxxoooooox

www.rsc.org/

Rebecca L. Agapov[a], Jonathan B. Boreyko[a,b], Dayrl P. Briggs[a], Bernadeta R. Srijanto[a,c], Scott T. Retterer[a], C. Patrick Collier[a], and Nickolay V. Lavrik[a]*

Arrays of tilted pillars with characteristic heights spanning from hundreds of nanometers to tens of micrometers were created using wafer level processing and used as Leidenfrost ratchets to control droplet directionality. Dynamic Leidenfrost droplets on the ratchets with nanoscale features were found to move in the direction of the pillar tilt while the opposite directionality was observed on the microscale ratchets. This remarkable switch in the droplet directionality can be explained by varying contributions from the two distinct mechanisms controlling droplet motion on Leidenfrost ratchets with nanoscale and microscale features. In particular, asymmetric wettability of dynamic Leidenfrost droplets upon initial impact appears to be the dominant mechanism determining their directionality on tilted nanoscale pillar arrays. By contrast, asymmetric wetting does not provide a strong enough driving force compared to the forces induced by asymmetric vapour flow on arrays of much taller tilted microscale pillars. Furthermore, asymmetric wetting plays a role only in the dynamic Leidenfrost regime, for instance when droplets repeatedly jump after their initial impact. The point of crossover between the two mechanisms coincides with the pillar heights comparable to the values of the thinnest vapor layers still capable of cushioning Leidenfrost droplets upon their initial impact. The proposed model of the length scale dependent interplay between the two mechanisms points to the previously unexplored ability to bias movement of dynamic Leidenfrost droplets and even switch their directionality.

Introduction

In the Leidenfrost regime, a droplet placed onto a hot surface levitates on a thin cushion of its own vapour.[1-3] Usually, the vapour flowing between the substrate and a droplet in this state follows a symmetric path and leads to minimal friction and reduced heat transfer.[4] Structuring of surfaces can be used to tune the heat transfer between the droplet and the surface as well as to bias the droplet movement to either induce directionality or halt the motion. Microscale,[5] nanoscale,[6] and micro-nano hierarchical[7-9] surface features have been employed to tune the heat transfer and alter the critical Leidenfrost temperature. Microscale crenelations, *i.e.* square ridges, have been used to increase the drag and trap Leidenfrost droplets, therefore arresting droplet motion.[10] Surfaces with periodic asymmetric saw-tooth profiles spanning micrometer to millimeter scales are known to enable the directional self-propulsion of Leidenfrost droplets.[11] Various mechanisms have been proposed to explain such a directional self-propulsion, commonly referred to as the *Leidenfrost ratchet* effect. These include a thermal creep mechanism driven by a temperature gradient,[12] a "jet pack" effect where the droplet is propelled in the opposite direction of the vapour flow,[13] and a viscous mechanism where the vapour drags the droplet in the same direction as its rectified flow.[11, 14-18]

On microscale and millimeter-scale Leidenfrost ratchets, droplets move against the feature tilt.[11, 14-18] Recently, arrays of approximately 300 nm tall tilted nanopillars were investigated. These surfaces exhibited only random motion of Leidenfrost droplets during steady state motion. However, droplet directionality in the *same* direction as the feature tilt was observed when the droplets dynamically impacted the nanostructured surface.[19] The proposed mechanism explaining the unusual directionality of these nanoscale ratchets is the asymmetric wetting of the substrate during droplet impact, which provides momentum for a directional rebound in the same direction as the feature tilt. The key to directionality at the nanoscale is *partial* liquid-solid contact, known as transition boiling,[20] upon droplet impact. This partial contact between the droplet and the substrate is facilitated by the concave bottom profile of a Leidenfrost droplet.[21, 22] It was shown previously that the underlying vapour film can thin to several hundred nanometers near the edges of the droplet during impact.[23] It is reasonable to assume that depending on the balance between the downward force and vapor pressure, brief contact between the droplet and the tops of the pillars is possible at the droplet perimeter during impact. Indeed, partial liquid-solid contact has been harnessed as a means of nanopatterning or nanocoating a substrate[24, 25] as well as a method to improve droplet transport by deflecting the trajectory of droplets at lower Leidenfrost temperatures.[26, 27] Partial contact between droplets

and microstructured superhydrophilic surfaces at slightly elevated temperatures has even enabled droplet stabilization under static conditions.[28]

Although the idea of intermittent contact between the surface and a Leidenfrost droplet may be perceived as being contradictory to the very definition of the classical Leidenfrost effect, it is clearly within a broader range of dynamic Leidenfrost phenomena.[4] Here we seek to identify a practical means of controlling the interplay between wetting and vapour flow phenomena in the dynamic Leidenfrost regime and determine the crossover point between the two mechanisms controlling droplet directionality. More specifically, we fabricate tilted pillar arrays (TPAs) at several different length scales of height to examine how the dominant mechanism controlling droplet directionality depends on the length scale and, more specifically, the height of the features comprising the surface texture. Furthermore, the behaviour of Leidenfrost droplets on microscale TPAs is compared to the behaviour of Leidenfrost droplets on microscale tilted ridge arrays (TRAs) to determine if the continuity of the surface structure in the direction perpendicular to droplet motion affects the droplet directionality. The findings reveal that surface wettability strongly influences the dynamic behaviour of Leidenfrost droplets when impacting nanoscale surface structures, however, the vapour flow mechanism dominates in the case of larger microscale surface features. Broadly, these results will be useful for tuning the wettability and droplet interaction on 3D micro- and nanostructures.

Experimental

Fabrication of Nanoscale Arrays[19]

A lithography free patterning strategy was used to create arrays of nanoscale pillars with large total areas.[29-32] A 5 nm to 15 nm thick layer of platinum (Pt) was deposited onto a single side polished single crystal silicon (Si) wafer (100) with 100 nm of thermally grown silicon oxide (SiO_2) using physical vapour deposition in a vacuum evaporator equipped with an electron gun source (Thermonics Laboratory, VE-240). This is shown schematically in Figure 1a. Wafers with a Pt coating were then thermally processed at ≈ 850°C for 8 seconds in a mixture of argon and hydrogen (10:1) at a pressure of 735 Torr in a cold wall furnace (Easy Tube 3000, First Nano, Ronkonkoma, NY) equipped with a radiative heat source set to its maximum power (22 kW). The resulting dewet Pt layer served as a mask during anisotropic reactive ion etching (RIE) of the SiO_2 and Si.[29-32] Glancing-angle reactive ion etching (RIE)[19] was carried out in an Oxford PlasmaLab system (Oxford Instruments, UK) with the wafer sitting on an aluminum holder bent to an angle of 70° relative to the surface of a silicon carrier wafer. A perfluorinated oil (Fomblin® 25/5) was placed between the wafer and the aluminum holder to ensure uniform heat flux during etching. The 100 nm of SiO_2 was etched in a mixture of C_4F_8 and O_2 at flow rates of 45 sccm and 2 sccm, respectively, at 15°C, 7 mTorr for 55 s. The anisotropic etching of Si was carried out at 10 mTorr in a SF_6:C_4F_8:Ar mixture defined by respective flow rates of 56, 25, and 5 sccm. Organic contaminants encountered during fabrication were removed from the nanopillar arrays with an O_2 plasma, resulting in superhydrophilic surfaces. The nanopillar dimensions and tilt angle were determined using a scanning electron microscope (Carl Zeiss, Merlin).

Fabrication of Microscale and Low Aspect Ratio Arrays

Photolithographic patterning was used to create arrays of microscale pillars. A single side polished single crystal Si wafer (100) with 100 nm of thermally grown SiO_2 was used as a starting material. A 0.7 μm thick film of a negative photoresist (NFR, Doe & Ingalls of North Carolina) was used to form an array of squares or rectangles that were 10 μm or 40 μm in diameter. The square features were used to form micropillars while the rectangles were used to form microridges. After exposure, the photoresist was developed using CD-26. The resulting patterns were etched with glancing-angle RIE. The 100 nm of SiO_2 was etched using a mixture of C_4F_8 and O_2 at flow rates of 45 sccm and 2 sccm, respectively, at 15 °C, 7 mTorr for 55 s. The anisotropic etching of Si was performed with Bosch etching. The Bosch etching consists of sequential deposition and etch steps. The deposition step has a mixture of SF_6 and C_4F_8 at flow rates of 1 sccm and 140 sccm, respectively, at 15 °C, 20 mTorr for 4 s. The etch step has a mixture of SF_6 and C_4F_8 at flow rates of 120 sccm and 1 sccm, respectively, at 15 °C, 20 mTorr for 5 s. The number of iterations determines the etch depth and therefore feature height. After the desired feature height was obtained, the photoresist mask and any organic contaminants encountered during fabrication were removed with an O_2 plasma, resulting in superhydrophilic or hydrophilic surfaces.

Smaller 1 μm to 3 μm diameter circular features were also patterned using a double layer of LOR™ A (Micro Chem) under a positive photoresist (MEGAPOSIT™ SPR™ 955-CM, The Dow Chemical Company). After development, chromium was deposited into the circular holes. The excess photoresist and metal was removed using an acetone bath followed by n-methyl-2-pyrrolidone (70°C, 20 min). The metal pattern was etched with glancing-angle RIE following the same recipes used for the larger diameter microscale arrays. After etching, the metal mask was removed using a chromium photomask etchant (Cr-145) bath for 2 min. An O_2 plasma was used to remove any organic contaminants encountered during fabrication.

Leidenfrost Experiments

Droplet impact and motion experiments were conducted on all of the TPAs, LAR-TPAs, and TRAs. These experiments were performed with deionized water on a leveled hot plate and a high speed camera (EPIX® X-Cap LTD V3.7, Sun Microsystems, Inc.) to record the droplet trajectory and velocity. The temperature was measured with a spot check surface thermometer (PTC Instruments, Model 573C). Droplets of a constant volume (8 μL) were dispensed with a syringe pump (Harvard Apparatus, Pump II Pico Plus Elite) leading to droplets with diameters of 2.5 mm. The height that the droplet was released from was controlled using a micrometer to alter the needle height connected to the syringe pump. The impact velocity for a droplet was obtained by measuring the vertical distance the droplet travelled between the two successive camera frames just prior to impact. Horizontal droplet trajectory and velocity was obtained by analyzing the recorded videos (1019 frames per second) with ImageJ (NIST, Version 1.45r) and monitoring the centroid position of the droplet in each successive frame using thresholding. At least five droplets were tracked for each surface at each temperature to obtain the average velocities presented.

Wetting at Room Temperature

The wetting characteristics at ambient temperature were obtained with a goniometer (Ramé-Hart Instrument Co., Model 590 F4 series with DROPimage Advanced V2.5) recording at 30 frames per second. The spreading of five 1.5 μL droplets was analyzed to obtain an average.

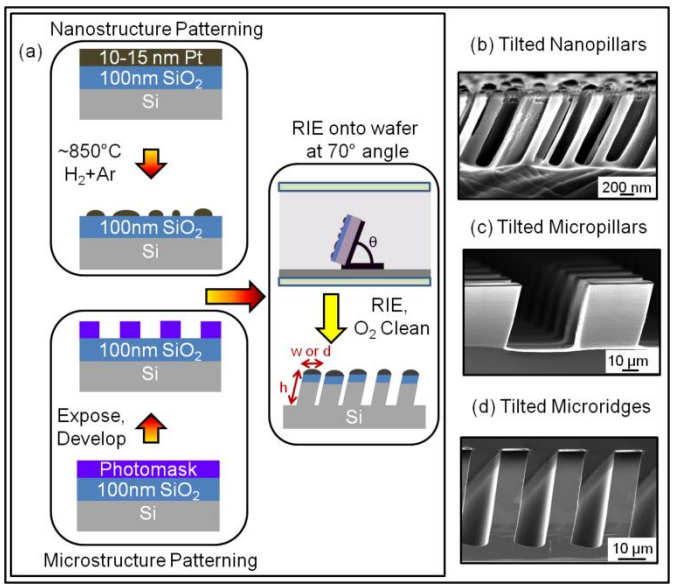

Fig. 1. (a) Fabrication sequence used in the present study to create tilted arrays. Nanostructures were masked with a thin film of platinum that was annealed in H_2:Ar at ≈ 850 °C. This leads to metal dewetting and the formation of circular Pt islands that serve as an etch mask. Microstructures were masked with photolithography using either a positive or negative resist. Reactive ion etching (RIE) of a masked wafer tilted at 70° relative to the carrier wafer resulted in tilted arrays of the masked features. The tilted arrays were then cleaned in an oxygen plasma to remove any organic contaminants encountered during fabrication. The measured width (w) or diameter (d) and height (h) are shown schematically. Representative cross-sectional scanning electron microscope images of a (b) nanoscale tilted pillar array, (c) microscale tilted pillar array, and (d) microscale tilted ridge array.

Results and discussion

Droplets placed onto isotropically structured surfaces are symmetric in shape. Adding channels/grooves,[33-36] or asymmetry[37-40] to the surface creates local energy barriers that cause preferential droplet spreading. Here, novel surface textures in the form of arrays of asymmetric, tilted pillars and tilted ridges were fabricated to control the surface wettability. Initially the diameters of the structures were adjusted while holding the aspect ratios constant within an order of magnitude to ensure stability of the structures under dynamic testing conditions. Representative images of a final nanoscale TPA, a microscale TPA, and a microscale TRA are shown in Figure 1b-d. To ensure that changes in the feature diameter did not significantly alter the results, low aspect ratio tilted pillar arrays (LAR-TPA) were also fabricated where the microscale diameter was held constant but the height was varied.

The effect of the asymmetric geometry of the TPAs and the TRAs on liquid spreading behavior was first assessed at room temperature. On the entire series of TPAs (micro- and nanoscale), a deionized water droplet spreads preferentially in the direction of the pillar tilt, with spreading ratios ranging from 1.5:1 to 2.5:1, as shown in Table 1. A representative image of droplet spreading behaviour is included in the Supporting Information. The final apparent contact angle (θ*) of an irreversibly impaled water droplet on all length scales of TPAs was θ* < 10°, indicating that the surfaces were superhydrophilic at room temperature.[41, 42] This preferential spreading of the water droplet in the direction of the pillar tilt is in agreement with prior reports on tilted pillars.[39, 43, 44] On the TRAs, a deionized water droplet sits symmetrically on top of the ridges (initial θ* = 110°) and spreads preferentially down the valleys between the ridges. Due to the fact that no preferential spreading occurred in the direction perpendicular to the channels, no spreading parameters are given for the TRAs. Droplet spreading on the TRAs took several seconds, after which time the droplet had a final θ* < 10°.

After it was confirmed that all of the TPAs induced asymmetric wetting preferentially in the direction of the pillar tilt at room temperature, the surface temperature of the arrays was increased to investigate droplet behavior in the Leidenfrost regime. The first test was to ensure that the gaps between the pillars did not alter Leidenfrost droplet behavior. To compare the effect of structure continuity, droplet behavior on microscale TPAs was compared to droplet behavior on microscale TRAs. The major distinction between the two surface features is that the pillars are discontinuous in the direction perpendicular to droplet motion whereas the ridges are continuous. These continuous ridges are of similar geometry to conventional Leidenfrost ratchets, which use

Table 1. Characterization of the tilted pillar array (TPA), tilted ridge array (TRA), and low aspect ratio tilted pillar array (LAR-TPA) substrates used. Height is measured from the substrate along the length of the pillar, as shown schematically in Figure 1a.

Surface	Average Diameter (or Width)[a] (μm)	Average Height[a] (μm)	Center to Center Spacing (μm)	Aspect Ratio	Spreading Ratio[b]	Dynamic Leidenfrost Temperature (C)
TPA-1	0.10 (± 0.03)	0.3 (± 0.1)	0.20 (± 0.05)	3	1.5 : 1	340° (± 15°)
TPA-2	0.20 (± 0.06)	1.1 (± 0.2)	0.32 (± 0.05)	6	2.5 : 1	360° (± 15°)
TPA-3	1.0 (± 0.1)	1.6 (± 0.2)	3.5 (± 0.2)	2	1.6 : 1	340° (± 10°)
TPA-4	3.2 (± 0.5)	2.5 (± 0.6)	5 (± 1)	1	1.5:1	335° (± 10°)
TPA-5	3.2 (± 0.5)	5.1 (± 0.4)	5 (± 1)	2	1.5:1	335° (± 10°)
TPA-6	9.5 (± 0.5)	40 (± 5)	20 (± 1)	4	1.9 : 1	310° (± 10°)
TPA-7	39 (± 0.5)	39 (± 4)	80 (± 1)	1	1.8 : 1	335° (± 10°)
LAR-TPA-1	11 (± 0.5)	0.3 (± 0.1)	20 (± 1)	0.03	1.4:1	340° (± 10°)
LAR-TPA-2	11 (± 0.5)	1.4 (± 0.3)	20 (± 1)	0.1	1.2 : 1	340° (± 10°)
TRA-1	10 (± 0.5)	32 (± 5)	20 (± 1)	3	-	335° (± 10°)
TRA-2	38 (±0.5)	44 (± 4)	80 (± 1)	1	-	335° (± 10°)

(a) Measured from SEM images.
(b) Spreading with the feature tilt : spreading against the feature tilt at room temperature.

Journal Name RSCPublishing

ARTICLE

a continuous saw-tooth pattern.[11, 13, 18] It is possible that the gaps in the TPAs studied here may provide an additional escape path for the vapour flow compared to the continuous structures which may affect directional rectification of the vapour. However, no substantial difference was observed between the microscale TPAs and the microscale TRAs of similar height, as shown in Figure 2. On all four of these surfaces, droplets impact the surface, spread symmetrically in the film boiling regime, and then travel in the direction opposite to the feature tilt. Average horizontal velocities on the TPAs were slightly larger than those of the TRAs, but were within the same order of magnitude. Due to the fact that the microscale TRAs had no preferential wetting in the direction of the feature tilt at room temperature, no preferential wetting is expected in the direction of the feature tilt on nanoscale TRAs.[36, 37] Therefore, nanoscale TRA structures are not expected to introduce any preferential directionality in the Leidenfrost regime and were not investigated.

On TPA-1 and TPA-2, *i.e.* nanoscale pillar features, no preferential directionality was observed when the droplets were deposited gently onto the structured surface in the film boiling regime. With gentle deposition, these droplets moved randomly on the surface. The intervening vapour film between the droplet and the surface has been experimentally measured to be on the order of 10 μm[2, 21] thick under gentle deposition conditions. This is too thick to allow for any liquid-solid contact at the tops of the nanopillars. This prevents asymmetric wetting of the surface and, therefore, a directional rebound of the droplet. In contrast to the droplet behavior on the nanostructured surfaces, droplets placed gently onto TPA-4 through TPA-7, *i.e.* microscale pillar features, immediately self-propelled in the direction opposite to the feature tilt. This immediate self-propulsion is in agreement with previous reports of traditional Leidenfrost ratchets driven by vapour rectification.[11, 13, 18, 26] On these surfaces the features are large enough to rectify the 10 μm[(2, 21)] thick vapour layer to direct the droplet's motion.

To better compare droplet directionalities observed on the various surfaces, droplet characteristics were analyzed at the same Weber number (*We*) and at the same surface temperature. The Weber number compares inertial effects to the surface tension of a droplet:

$$We = \frac{\rho V^2 D}{\sigma} \quad (1)$$

where ρ is the density of the liquid (958 kg/m^3 at 100 °C for water), *V* is its impact velocity, *D* is the droplet diameter, and σ is the surface tension (58 N/m at 100 °C for water). The directional velocities of water droplets on all of the structured surfaces, shown in Figure 2, were compared at 350 °C and *We* ≈ 2. Under these impact conditions, droplets accelerated at rates of ~1-2 m/s^2 on average and reached average horizontal velocities up to 50 mm/s. A representative position vs. time plot is shown in the Supporting Information. At this *We*, droplets impacted the nanostructured surfaces in the transition boiling regime. In this regime, droplets asymmetrically wet the nanostructured surface upon impact, evident by the slight film spraying that occurs upon impact, and experience a directional rebound.[19] This leads to a preferential droplet directionality that coincides with the feature tilt. For these data, no droplets that impacted the surface in a nucleate boiling regime were included in the velocity analysis, *i.e.* where the liquid-solid contact was so violent that the vapour pressure increased abruptly, causing explosive ejection of tiny droplets due to the venting of vapour bubbles. To construct this plot, a coordinate system was used to track the droplet directionalities on substrates where all of the surface structures were tilted to the left. The center of impact was used as the origin, with directionality coinciding with the feature tilt having a negative velocity value and directionality against the feature tilt having a positive velocity value. The horizontal velocity for a single droplet was obtained from the rate at which the droplet moved over a distance of approximately 5 mm after initial impact, taking directionality into account. The data presented in Figure 2 are the average velocity observed from a minimum of five droplets with the vertical error bars marking the range of velocities observed.

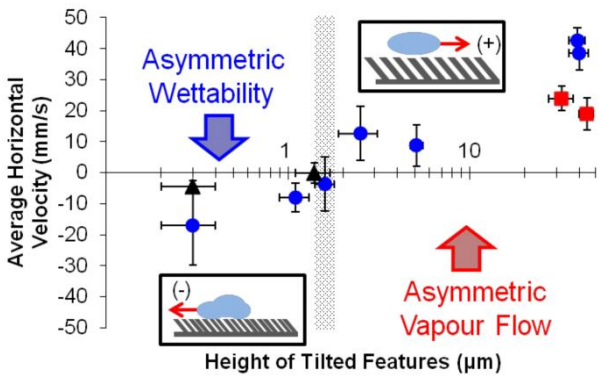

Fig. 2. Average horizontal velocity as a function of height of the tilted features. Negative velocity values indicate directionality that coincides with the feature tilt while positive velocity values indicate directionality against the feature tilt. All data were acquired with the surfaces held at 350 °C and *We* ≈ 2. Droplets on the tilted pillar arrays (TPAs) (circles) and low aspect ratio tilted pillar arrays (LAR-TPA) (triangles) change from an asymmetric wettability mechanism for directionality, shown schematically in the bottom inset, to a vapour flow mechanism, shown schematically in the top inset. This transition occurs when the feature height reaches the microscale and is marked with hash marks to guide the eye. No difference in directionality is observed between microscale TPAs and microscale tilted ridge arrays (squares). Error bars are the range of velocities observed from several droplets.

On TPA-1 and TPA-2, only directionality that coincides with the tilt of the features was observed. This directionality was observed from droplets that dynamically impacted the surface in the transition boiling regime, as evident from the film spraying observed during impact (Figure 3a), and spread asymmetrically. The directional rebound from the asymmetric spreading provided momentum that kept the

droplet moving in the direction of the pillar tilt. On TPA-1, the directional rebound was observed to be 21° (± 6°) off normal, while the directional rebound on TPA-2 was observed to be 5° (± 2°) off normal. On TPA-4 through TPA-7, droplets were observed to self-propel in the direction opposite to the feature tilt (Figure 3b). Representative videos are contained in Supporting Information. It is remarkable that a change in directionality is observed between the analogous nanoscale and microscale TPAs despite the fact that all of these TPAs are superhydrophilic with droplet spreading preferentially in the direction of the pillar tilt at room temperature. This clearly indicates that asymmetric wetting is not a strong enough driving force compared to the force from directional vapour flow to control droplet directionality on larger microscale features. The directionality observed on TPA-4 through TPA-7 is consistent with that reported for saw-tooth shaped Leidenfrost ratchets ranging from the microscale[16] to the millimeter scale[11, 13, 18] where the droplet directionality was achieved via the rectification of vapour flow. [11, 13-17]

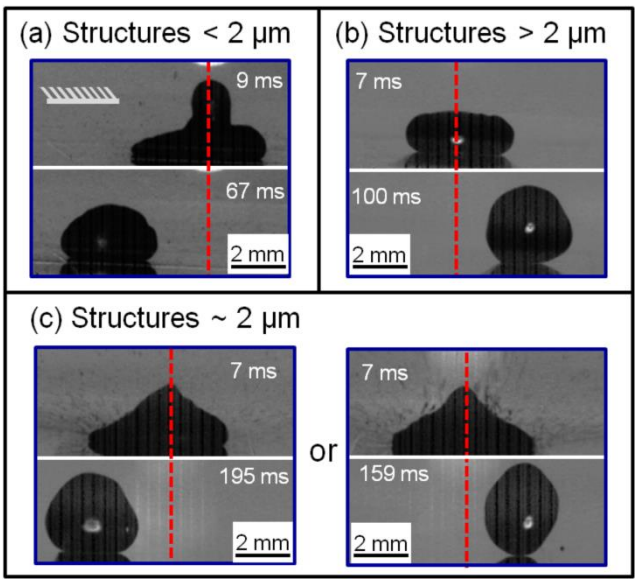

Fig. 3. Representative droplet impact and directionality images at 350 °C and *We* ≈ 2 on (a) nanoscale tilted pillar arrays (TPAs), (b) tall microscale TPA and tilted ridge arrays, and (c) short microscale TPA. Brief contact is observed for the nanoscale as well as the short microscale TPAs, as evident from the spray boiling observed during initial impact. Only film boiling is observed for the large microscale TPAs. The time stamps are times after initial droplet contact with the structured surface. All surface features are tilted to the left, as shown by the schematic in (a).

Intriguingly, droplets placed onto the surface structured with short microscale features (TPA-3) exhibited no preferential directionality at a temperature of 350 °C and *We* ≈ 2, *i.e.* droplets moving either in the same direction as the feature tilt or against it (Figure 3c). Since droplets impacting this surface at 350 °C and *We* ≈ 2 do not have a preferential directionality, it is therefore of interest to determine if the experimental parameters can be tuned to control the directionality. The droplet interaction with the surface was modified in two ways: firstly, by holding *We* constant and changing the surface temperature, and secondly, by holding the temperature constant and changing *We* by varying the height from which the droplets are released. Both of these methods are expected to change the thickness of the vapour layer between the droplet and the surface.[5] Models exist that predict the scaling behavior of the vapour film thickness underneath a Leidenfrost droplet.[5, 45] In these models, the thickness of the vapor layer scales with both *We* and surface temperature. However, these models tend to overestimate the absolute thickness of the vapour film during droplet impact compared to experimentally measured values. The thickness of the vapour layer at impact has been experimentally determined[5, 23] to be several hundred nanometers at the droplet edge to approximately 2 μm near the center for a droplet of similar diameter to those used here impacting the surface at a *We* of 3.5 and surface temperature of 350 °C. We therefore relate the results obtained here to the experimentally measured thickness of the vapour film during impact, which correlates well to the height of the surface features on TPA-3.

When the temperature is increased but the *We* stays the same, shown in Figure 4a, a switch in directionality is observed for droplets impacting TPA-3. At 300 °C, all of the droplets interact with the surface during impact, spread asymmetrically, then rebound and travel in the direction of the pillar tilt. As the temperature is increased, the thickness of the vapour layer underneath the droplet increases, which in turn, reduces the likelihood of any direct interaction of the droplet with the surface.[2] This leads to a shift in the balance between the asymmetric wettability mechanism and the vapour flow mechanism. At 375 °C, the vapour flow mechanism dominates the asymmetric wettability mechanism, resulting in all of the droplets travelling against the pillar tilt.

Similar trends are observed when the temperature is held constant but *We* is varied, as shown in Figure 4b. When the surface is held at 350 °C, the droplets moved randomly at *We* < 2. This occurs as a result of the thicker intervening vapour layer minimizing any interaction of the droplet with the structured surface. However, at higher *We*, the droplets impact the surface more violently and thin the intervening vapour film to the point when a brief partial contact between the droplet and the surface becomes possible. Indeed, the resulting motion of the droplets in the same direction as the feature tilt can be explained by asymmetric wetting of the surface. When the surface is held at 375 °C, the droplets move randomly at *We* < 2, however, at *We* in the range of 2 to 5, all of the droplets move in the direction *opposite* to the feature tilt, consistent with the vapour rectification mechanism. Further thinning of the vapour layer upon droplet impact at *We* > 5 increases the contribution from the asymmetric wettability mechanism. A loss of preferential directionality under these conditions confirms that the opposing forces associated with each of the two mechanisms cancel each other in these conditions. This loss of preferential directionality is observed in the data as an average velocity crossing zero. These results indicate that it is the delicate balance between the gravitational forces, the cushioning vapor action and intermittent wetting of TPA surface by dynamic Leidenfrost droplets that controls the droplet directionality. When the surface feature height is comparable to the vapour film thickness at impact, the vapour rectification mechanism becomes the dominant mechanism controlling droplet directionality. This transition occurs at a surface feature height of approximately 2 μm for the droplet impact conditions studied here. This demonstrates that tuning the thickness of the droplet's vapour film during impact onto short microscale features enables precise tuning of droplet dynamics by biasing the droplet to follow either the vapour flow mechanism or the asymmetric wettability mechanism.

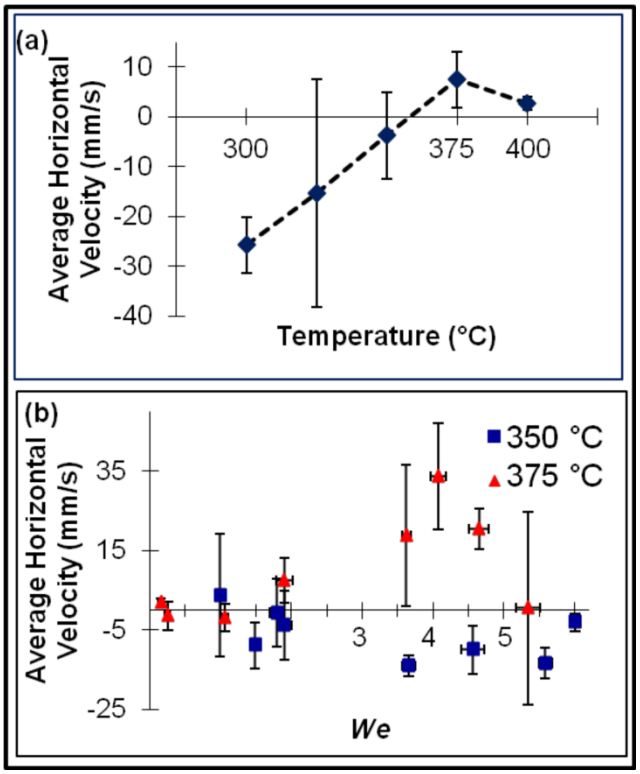

Fig. 4. (a) Average horizontal velocity as a function of temperature on TPA-3 at *We* ≈ 2. (b) Average horizontal velocities of droplets on TPA-3 as a function of *We* at temperatures of 350 °C (squares) and 375 °C (triangles).

To disentangle the effect of feature diameter from feature height, LAR-TPAs were investigated. These arrays had microscale diameters and aspect ratios less than one. The LAR-TPAs exhibited asymmetric wettability (Table 1) at room temperature similar to their larger aspect ratio counterparts. The LAR-TPAs were hydrophilic with measured $\theta^* = 52°$ (± 6°) for LAR-TPA-1 and $\theta^* = 43°$ (± 5°) for LAR-TPA-2 at room temperature. This change in hydrophilicity compared to the other TPAs is expected due to the decreased surface roughness with the lower aspect ratio features.[46] When the surface temperature was increased to the Leidenfrost regime, droplets impacting LAR-TPA-1 moved controllably in the same direction as the feature tilt (Figure 2). This directionality is a result of the droplets asymmetrically wetting the nanoscale features during impact and undergoing a directional rebound observed to be 5° (± 2°) off normal. Droplets impacting LAR-TPA-2 moved randomly. As with TPA-3, the surface features here are approximately the height of the droplet's vapour film during impact. This leads to competition between the asymmetric wettability mechanism and the vapour flow mechanism and therefore a lack of control over droplet directionality under these impact conditions. These data confirm that changing the diameter of surface features with the same length scale of height does not significantly alter the droplet directionality observed in the Leidenfrost regime.

Conclusions

In conclusion, arrays of tilted pillars ranging in height from hundreds of nanometers to tens of microns were fabricated to control Leidenfrost droplet directionality. The characteristic direction of the droplets was observed to switch from movement coinciding with the surface tilt on the nanoscale ratchets to movement against the feature tilt on the microscale ratchets. It is remarkable that a change in directionality in the Leidenfrost regime is observed on surfaces of similarly shaped features that all exhibit asymmetric wettability with the same preferential spreading direction at room temperature. This notable change in directionality occurs due to varying contributions from the two distinct mechanisms controlling droplet directionality in the Leidenfrost regime. In particular, asymmetric wettability of dynamic Leidenfrost droplets upon impact appears to be the dominant mechanism controlling directionality on tilted nanoscale pillar arrays. However, asymmetric wetting does not provide a strong enough driving force compared to the forces induced by asymmetric vapour flow on arrays of much taller tilted microscale pillars. This crossover occurs when the height of the surface features coincides with the values of thinnest vapor layers still capable of cushioning Leidenfrost droplets upon their initial impact. No significant differences were observed between microscale arrays of tilted ridges and tilted pillars indicating that the gap regions between the pillars do not significantly alter the vapour flow through the 3D structure. The ability to bias a droplet to follow either the vapour flow mechanism or the asymmetric wettability mechanism by merely tuning the height of asymmetric surface features enables precise tuning of droplet dynamics and directionality.

Acknowledgements

This research was conducted at the Center for Nanophase Materials Sciences, which is sponsored at Oak Ridge National Laboratory by the Division of Scientific User Facilities, U.S. Department of Energy.

Notes and references

[a] Center for Nanophase Materials Sciences, Oak Ridge National Laboratory, Oak Ridge, TN, 37831 (USA) E-mail: lavriknv@ornl.gov
[b] Bredesen Center for Interdisciplinary Research, University of Tennessee, Knoxville, TN 37996 (USA)
[c] Department of Materials Science and Engineering, University of Tennessee, Knoxville, TN, 37996 (USA)

†Electronic Supplementary Information (ESI) available: representative room temperature wetting images and videos of droplet motion on the various structured surfaces. See DOI: 10.1039/b000000x/

1. J. G. Leidenfrost, *Int. J. Heat Mass Transfer*, 1966, **9**, 1153.
2. A. L. Biance, C. Clanet and D. Quéré, *Phys. Fluids*, 2003, **15**, 1632.
3. A. L. Biance, F. Chevy, C. Clanet, G. Lagubeau and D. Quéré, *J. Fluid Mech.*, 2006, **554**, 47.
4. D. Quéré, *Annu. Rev. Fluid Mech.*, 2013, **45**, 197.
5. T. Tran, H. J. J. Staat, A. Susarrey-Arce, T. C. Foertsch, A. van Houselt, H. Gardeniers, A. Prosperetti, D. Lohse and C. Sun, *Soft Matter*, 2013, **9**, 3272.
6. S. H. Kim, H. S. Ahn, J. Kim, M. Kaviany and M. H. Kim, *Appl. Phys. Lett.*, 2013, **102**, 233901.
7. H. M. Kwon, J. C. Bird and K. K. Varanasi, *Appl. Phys. Lett.*, 2013, **103**, 201601.
8. C. Kruse, T. Anderson, C. Wilson, C. Zuhlke, D. Alexander, G. Gogos and S. Ndao, *Langmuir*, 2013, **29**, 9798.

9. H. Kim, B. Truong, J. Buongiorno and L. W. Hu, *Appl. Phys. Lett.*, 2011, **98**, 083121.
10. G. Dupeux, M. Le Merrer, C. Clanet and D. Quéré, *Phys. Rev. Lett.*, 2011, **107**, 114503.
11. H. Linke, B. J. Aleman, L. D. Melling, M. J. Taormina, M. J. Francis, C. C. Dow-Hygelund, V. Narayanan, R. P. Taylor and A. Stout, *Phys. Rev. Lett.*, 2006, **96**, 154502.
12. A. Wurger, *Phys. Rev. Lett.*, 2011, **107**, 164502.
13. G. Lagubeau, M. Le Merrer, C. Clanet and D. Quéré, *Nature Phys.*, 2011, **7**, 395.
14. G. Dupeux, M. Le Merrer, G. Lagubeau, C. Clanet, S. Hardt and D. Quéré, *Europhys. Lett.*, 2011, **96**, 58001.
15. T. Baier, G. Dupeux, S. Herbert, S. Hardt and D. Quéré, *Phys. Rev. E*, 2013, **87**, 021001.
16. Á. G. Marín, D. A. del Cerro, G. R. B. E. Römer, B. Pathiraj, A. J. Huis In't Veld and D. Lohse, *Phys. Fluids*, 2012, **24**, 122001.
17. S. Hardt, S. Tiwari and T. Baier, *Phys. Rev. E*, 2013, **87**, 063015.
18. T. R. Cousins, R. E. Goldstein, J. W. Jaworski and A. I. Pesci, *J. Fluid Mech.*, 2012, **696**, 215.
19. R. L. Agapov, J. B. Boreyko, D. P. Briggs, B. R. Srijanto, S. T. Retterer, C. P. Collier and N. V. Lavrik, *ACS Nano*, 2014, **8**, 860.
20. W. S. Bradfield, *Ind. Eng. Chem. Fundamen.*, 1966, **5**, 200.
21. J. C. Burton, A. L. Sharpe, R. C. A. van der Veen, A. Franco and S. R. Nagel, *Phys. Rev. Lett.*, 2012, **109**, 074301.
22. D. J. E. Harvie and D. F. Fletcher, *Int. J. Heat Mass Transfer*, 2001, **44**, 2643.
23. T. Tran, H. J. J. Staat, A. Prosperetti, C. Sun and D. Lohse, *Phys. Rev. Lett.*, 2012, **108**, 036101.
24. M. Elbahri, D. Paretkar, K. Hirmas, S. Jebril and R. Adelung, *Adv. Mater.*, 2007, **19**, 1262.
25. R. Abdelaziz, D. Disci-Zayed, M. K. Hedayati, J. H. Pohls, A. U. Zillohu, B. Erkartal, V. S. K. Chakravadhanula, V. Duppel, L. Kienle and M. Elbahri, *Nature Comm.*, 2013, **4**, 2400.
26. J. T. Ok, E. Lopez-Ona, D. E. Nikitopoulos, H. Wong and S. Park, *Microfluid. Nanofluid.*, 2011, **10**, 1045.
27. A. Grounds, R. Still and K. Takashina, *Sci. Rep.*, 2012, **2**, 720.
28. S. Adera, R. Raj, R. Enright and E. N. Wang, *Nature Comm.*, 2013, **4**, 2518.
29. S. Strobel, C. Kirkendall, J. B. Chang and K. K. Berggren, *Nanotechnology*, 2010, **21**, 505301.
30. R. L. Agapov, B. Srijanto, C. Fowler, D. Briggs, N. V. Lavrik and M. J. Sepaniak, *Nanotechnology*, 2013, **24**, 505302.
31. J. M. Lee and B. I. Kim, *Mater. Sci. Eng. A*, 2007, **449**, 769.
32. J. B. Boreyko, B. R. Srijanto, T. D. Nguyen, C. Vega, M. Fuentes-Cabrera and C. P. Collier, *Langmuir*, 2013, **29**, 9516.
33. Y. Chen, B. He, J. H. Lee and N. A. Patankar, *J. Colloid Interface Sci.*, 2005, **281**, 458.
34. H. Kusumaatmaja, R. J. Vrancken, C. W. M. Bastiaansen and J. M. Yeomans, *Langmuir*, 2008, **24**, 7299.
35. R. Seemann, M. Brinkmann, E. J. Kramer, F. F. Lange and R. Lipowsky, *P. Natl. Acad. Sci. USA*, 2005, **102**, 1848.
36. Y. Zhao, Q. Lu, M. Li and X. Li, *Langmuir*, 2007, **23**, 6212.
37. J. Y. Chung, J. P. Youngblood and C. M. Stafford, *Soft Matter*, 2007, **3**, 1163.
38. W. W. Wu, L. Cheng, S. Bai, Z. L. Wang and Y. Qin, *Adv. Mater.*, 2012, **24**, 817.
39. K. H. Chu, R. Xiao and E. N. Wang, *Nature Mater.*, 2010, **9**, 413.
40. N. A. Malvadkar, M. J. Hancock, K. Sekeroglu, W. J. Dressick and M. C. Demirel, *Nature Mater.*, 2010, **9**, 1023.
41. S. J. Kim, M. W. Moon, K. R. Lee, D. Y. Lee, Y. S. Chang and H. Y. Kim, *J. Fluid Mech.*, 2011, **680**, 477.
42. S. J. Kim, J. Kim, M. W. Moon, K. R. Lee and H. Y. Kim, *Phys. Fluids*, 2013, **25**, 092110.
43. X. M. Yang, Z. W. Zhong, E. Q. Li, Z. H. Wang, W. Xu, S. T. Thoroddsen and X. X. Zhang, *Soft Matter*, 2013, **9**, 11113.
44. A. Cavalli, M. L. Blow and J. M. Yeomans, *Soft Matter*, 2013, **9**, 6862.
45. C. T. Avedisian and J. Koplik, *Int. J. Heat Mass Transfer*, 1987, **30**, 379.
46. D. Quéré, *Ann. Rev. Mater. Res.*, 2008, **38**, 71.